https://doi.org/10.1016/j.orgel.2021.106216


# A Tris β-Diketonate Europium(III) Complex Based OLED Fabricated by Thermal Evaporation Method Displaying Efficient Bright Red Emission

**Rashid Ilmi,[a]* Danyang Zhang,[b] José D. L. Dutra,[c] Necmi Dege,[d] Liang Zhou,[b]* Wai-Yeung Wong,*[e] Paul R. Raithby*[f] and Muhammad S. Khan[a]***

[a]Department of Chemistry, Sultan Qaboos University, P. O. Box 36, Al Khod 123, Oman

[b]State Key Laboratory of Rare Earth Resource Utilization, Changchun Institute of Applied Chemistry, Chinese Academy of Sciences, Renmin Street 5625, Changchun 130022, People's Republic of China.

[c]Pople Computational Chemistry Laboratory, Department of Chemistry, UFS, 49100-000 São Cristóvão, Sergipe, Brazil.

[d]Ondkuz Mayıs University, Faculty of Arts and Sciences, Department of Physics, Samsun, Turkey.

[e]Department of Applied Biology and Chemical Technology, The Hong Kong Polytechnic University, Hung Hom, Kowloon, Hong Kong, People's Republic of China.

[f]Department of Chemistry, University of Bath, Claverton Down, Bath BA2 7AY, UK.

**E-mail addresses and ORCID ID of corresponding authors:**

Rashid Ilmi : rashidilmi@gmail.com; 0000-0002-5165-5977

Muhammad S. Khan : msk@squ.edu.om; 0000-0001-5606-6832

Liang Zhou : zhoul@ciac.ac.cn; 0000-0002-2751-5974

Wai-Yeung Wong : wai-yeung.wong@polyu.edu.hk; 0000-0002-9949-7525

Paul R. Raithby : p.r.raithby@bath.ac.uk; 0000-0002-2944-0662

**Abstract**: A new tris β-diketonate europium(III) complex [Eu(btfa)$_3$Py-Im] (**Eu-1**) (4,4,4-trifluoro-1-phenyl-1,3-butanedione (btfa) and 2-(2-pyridyl)benzimidazole (Py-Im)] has been synthesized and structurally characterized. A single crystal X-ray diffraction analysis shows that **Eu-1** is octacoordinated and the coordination sphere is composed of a $EuO_6N_2$ core with trigonal dodecahedral ($D_{2d}$) geometry. The photophysical properties of **Eu-1** were analysed in detail and with the help of the experimental PL data and theoretical modelling, energy transfer rates were calculated, and an energy transfer mechanism is proposed for **Eu-1**. The complex has been used as the emitting layer (EML) to fabricate organic light emitting diodes (OLEDs). Eight OLEDs, of which four single-EML and four double-EML with varying doping concentration, were fabricated *via* a thermal evaporation method using **Eu-1** as the EML. Under the optimum conditions a highly monochromatic bright red emission ($CIE_{x,y}$ = 0.640, 0.311) with brightness (B) = 896 cd/m$^2$, current efficiency ($\eta_c$) = 2.26 cd/A, power efficiency ($\eta_p$) = 1.92 lm/W and EQE = 1.6% at very low $V_{turn\text{-}on}$ = 3.4 V was obtained.

**Keywords**: Europium(III), 2-(2-pyridyl)benzimidazole, Photoluminescence, Energy transfer mechanism, Electroluminescence

## 1. Introduction

OLEDs are omnipresent in modern technology such as displays and lighting technologies owing to their excellent color quality, simple construction, low cost, environment-friendly nature, and energy-saving properties [1]. However, there remains a need to develop OLEDs with excellent color purity with sufficient photoluminescence (PL) efficiency for use in an extensive range of applications. Lanthanide complexes with organic ligands [2], and in particular trivalent europium(III) complexes with anionic β-diketones as primary antenna and neutral ancillary (N^N) ligand(s) [2d, 2e], could be excellent emitters in electroluminescent devices because of their inherent photophysical properties and pure red emissions. In order to obtain efficient organoeuropium complexes it is necessary to choose or design suitable ligand(s) with some important prerequisites such as ability to form thermally stable complexes, strongly absorbing in the region between 250 – 450 nm, a triplet state ($T_1$) above the $^5D_0$ emitting state (17,300 $cm^{-1}$) for efficient ligand-to-metal energy transfer (LMET) [3]. Thus, the search for existing and new ligands that can provide improved PL properties constitutes an ongoing research area.

An unsymmetrical fluorinated 4,4,4-trifluoro-1-phenyl-1,3-butanedione (btfa), with its compatible $T_1 \approx$ 21,400 $cm^{-1}$) [3b] is a good choice of primary antenna ligand. Indeed, we have recently demonstrated that this ligand is an excellent antenna ligand for Eu(III) in conjunction with neutral ancillary (N^N/O^O) ligands with the sensitization efficiency reaching 90% [4]. The nature of the ancillary ligands is also important in imparting desirable physical and chemical properties to the resultant europium complex. For example, the ancillary 'Py-Im' (2-(2-pyridyl)benzimidazole) ligand provides asymmetric coordination environment with a large bite angle between the N donors of the five-membered imidazolyl ring and six-membered pyridyl nitrogen with a well-placed $T_1 \approx$ 20,576 $cm^{-1}$) [5]. Huang et al, [6] have exploited these properties to synthesize a series of europium complexes with Py-Im and functionalized Py-Im ligands that have been used as EML to fabricate pure red emitting OLEDs with brightness (B) = 180 $cd/m^2$ at 18V and $\eta_p$ of 0.0056 lm/W at 10 V. Liang et al, [7] reported oxadiazole

functionalized Py-Im and the mixed-ligand europium complex [Eu(dbm)$_3$(Ox-Py-Im)] (Ox-Py-Im = 2-phenyl-5-(4-(4-(2-(pyridin-2-yl)-1H-benzo[d]imidazol-1-yl)butoxy)phenyl)-1,3,4-oxadiazole). The complex exhibited B = 322 cd/m$^2$ and current efficiency ($\eta_c$) = 1.9 cd/A at 21V. Zhang et al, [8] modified the ancillary ligand with the hole-transporting carbazole moiety and synthesized a new [Eu(dbm)$_3$(Car–Py-Im)] (dbm = dibenzoylmethanato and Car-Py-Im = 9-(5-(2-(pyridin-2-yl)-1H-benzo[d]imidazol-1-yl)pentyl)-4a,4b,8a,9a-tetrahydro-9H-carbazole) which, when incorporated into a device, gives a better hole-transport ability compared to the unsubstituted Py-Im complex. The complex displayed B = 200 cd/m$^2$ at 20 V and $\eta_c$ = 4.2 cd/A at 0.5 mA/cm$^2$. However, the EL performance of devices using the family of Py-Im complexes have very high operating voltages (10 – 21 V), which limits their use in real-life applications [6-9]. It is important to note that majority of the published research in this area is based on thenoyltrifluoroacetonate (tta) and dbm supported Eu(III) complexes and there are few reports of other β-diketone based Eu(III) complexes in the literature.[2d] Thus, the potential of other β-diketone ligand based complexes remains a relatively unexplored area of research. In the present work, we have incorporated the bfta and Py-Im ligands in the same complex and report the analysis and the detailed photophysical properties of newly synthesized [Eu(btfa)$_3$(Py-Im)] (**Eu-1**) complex (**Chart S1,** electronic supporting information [**ESI**]). The properties established include the measurement of lifetime ($\tau_{obs}$), photoluminescence quantum yield ($Q_{Eu}^{L}$), intrinsic quantum yield ($Q_{Eu}^{Eu}$), radiative ($A_R$) and nonradiative ($A_{NR}$) decay rates, sensitization efficiency ($\eta_{sen}$) and the energy transfer (ET) process. Finally, we have successfully employed **Eu-1** was as an emitter to fabricate single- and double-EML red-emitting EL devices.

## 2. Experimental Section

All chemicals used in the synthesis and in the OLED fabrication were purchased from commercial sources and were used without further purification unless otherwise specified. Solvents used in the experiments were dried and distilled prior to use. Elemental analysis of **Eu-1** was performed on a Euro EA−CHN Elemental Analyser. The Fourier transform infrared (FTIR) spectrum of the solid **Eu-1** was obtained using a Cary 630 FT-IR spectrometer in the

attenuated total reflectance (ATR) mode. The mass spectrum was obtained using a Bruker autoflex III smartbeam MALDI-TOF/TOF mass spectrometer. Thermal stability of **Eu-1** was determined by thermogravimetric analysis (TGA) and differential thermogravimetric analysis (DTA) in the temperature range between 50 and 800 °C under a dinitrogen atmosphere and recorded on TA instrument model SDTQ600.

### 2.1. Synthesis of [Eu(btfa)$_3$(Py-Im)] (Eu-1)

The complex [Eu(btfa)$_3$(Py-Im)] (**Eu-1**) was synthesized by dropwise addition of an ethanolic solution of Py-Im (0.120 g, 0.615 mmol) to an ethanolic solution of [Eu(btfa)$_3$($H_2O$)$_2$] [4a] (0.400 g, 0.615 mmol). The reaction mixture was stirred overnight at ambient temperature and left for slow solvent evaporation for a week, after which period the solvent was decanted and the powder was washed with ice-cold ethanol followed by hexane and dried in the air. Microanalysis: calculated for $C_{42}H_{27}EuF_9N_3O_6$: C, 50.82; H, 2.74; N, 4.23 %; found C, 51.05; H, 2.72; N, 4.30 %; ESI-MS$^+$ m/z: 778.1 for [Eu(btfa)$_2$Py-Im]; FT-IR (solid;cm$^{-1}$, **Fig. S1, ESI**) - $\nu$(N-H) ~ 3250; $\nu$(C=O) ~ 1604; $\nu$(C=C) ~ 1,532(m); melting point ($T_m$): 220 °C; decomposition temperature ($T_d$): 284 °C. Crystals of **Eu-1** suitable for single-crystal X-ray analysis were grown by slow evaporation from a mixed (50:50) dichloromethane ($CH_2Cl_2$) and acetonitrile (ACN) solution. The details are included in the electronic supporting information (**Section 1, ESI)**.

### 2.2. Spectroscopic measurements, photophysical parameters and computational Chemistry

Spectroscopic measurements of **Eu-**1 including optical absorption, excitation, emission spectra, decay profiles and absolute PLQY values were obtained at room temperature; details of the measurements have been reported previously [4a]. Optical absorption spectra were obtained using Varian Cary 50 spectrophotometer while excitation, emission spectra and decay profiles were recorded on an Edinburgh FS5 fluorimeter. The absolute PLQY values were determined using a calibrated integrating sphere on a C-9920-02 from Hamamatsu Photonic instrument. Photophysical parameters such as the Judd-Ofelt (J-O) parameters (

$\Omega_2$ and $\Omega_4$), $A_R$, $A_{NR}$ decay rates, radiative lifetime ($\tau_{rad}$), $Q_{Eu}^{Eu}$ and $\eta_{sen}$ were calculated using equations S1 – S7 (**Section 1.1, ESI**) and details are reported elsewhere [5]. To understand the energy transfer (ET) mechanism and to propose ET pathways in a given complex, it is necessary to obtain the theoretical ground state geometry of the complex in question. The optimized geometry was used to determine the singlet (S) and triplet (T) energy level, and $\Omega_2$ and $\Omega_4$ theoretical and calculations. The details of these calculations are included in **Section 2, ESI**.

### 2.3. Fabrication of EL devices and assessments of their EL performance

ITO coated glass with the sheet resistance of 10 Ω/sq was used as the anode substrate. Prior to film deposition, patterned ITO substrates were cleaned with detergent, rinsed in de-ionized water, and finally dried in an oven. All organic layers were deposited at a rate of 0.1 nm/s under high vacuum (≤ $3.0\times10^{-5}$ Pa). The doped EMLs were prepared by co-evaporating dopant and host material from two sources, and the doping concentration was modulated by controlling the evaporation rate of dopant. LiF and Al were deposited in another vacuum chamber (≤ $8.0\times10^{-5}$ Pa) at rates of 0.01 and 1.0 nm/s, respectively, without being exposed to the atmosphere. The thicknesses of these deposited layers and the evaporation rate of individual materials were monitored in vacuum with quartz crystal monitors. A shadow mask was used to define the cathode and make eight emitting dots with the active area of 9 $mm^2$ on each substrate. Current density-brightness-voltage (J-B-V) characteristics were measured by using a programmable brightness light distribution characteristics measurement system C9920-11 from Hamamatsu Photonic instrument. PL and EL spectra were measured with a calibrated Hitachi F−7000 fluorescence spectrophotometer and an Ocean Optics spectrophotometer.

## 3. Results and discussion

### 3.1. Synthesis, characterization and single crystal structure of Eu-1

The complex **Eu-1** was synthesized by the reaction of an equimolar ethanolic solution of $[Eu(btfa)_3(H_2O)_2]$ [4a] and Py-Im and was characterized by elemental analysis, FT-IR and ESI-

MS. The results are in agreement with the formula of **Eu-1** proposed in **Chart S1, ESI**. The solid-state structure of **Eu-1** was determined by single-crystal X-ray diffraction. **Eu-1** crystallises in the triclinic space group *P-1* (no. 2) with one independent molecule in the crystallographic asymmetric unit (structural parameters are included in **Tables S1 – S8**, **ESI**). Within the crystal structure the closest intermolecular contacts involve the N(3)-H(3) unit of the imidazole ring of the Py-Im ligand and O and F atoms of an adjacent btfa ligand [N(3)···O(2i) 3.009 Å, N(3)-H(3)···O(2i) 155.3°; N(3)···F(1i) 3.146(6) Å; N(3)-H(3)···F(1i) 127.2° (symmetry operator (i) 2-x, 2-y, 1-z).

The molecular structure is illustrated in **Fig. 1(a)** which includes selected bond parameters, while the ligand coordination environment around the central Eu atom is shown in **Fig. 1(b)**. The Eu atom is eight coordinate with the coordination sphere made up of the three pairs of oxygen donor atoms from the three bidentate btfa ligands and the two nitrogen donor atoms from the bidentate Py-Im ligand. The coordination geometry has been analysed using the *SHAPE 2.1* software package[10] which calculates continuous shape measures (CShMs) of a set of atomic positions, in this case the Eu centred $O_6N_2$ coordination sphere, relative to the vertices of a series of ideal reference polyhedra [11]. In this instance the coordination polyhedron is best described as a distorted trigonal dodecahedron. The calculated CShMs is compared with the values for the idealised trigonal dodecahedral and the square antiprismatic geometries, the two most common eight coordinate geometries, are shown in **Table S9, ESI**. A value of zero for the CShM would represent perfect agreement with the idealised polyhedron.

However, an inspection of the whole molecular structure as shown in **Fig. 1(a)** suggests that the molecular point group for the molecule is much lower than $D_{2d}$ since all four of the coordinated bidentate ligands are asymmetric in nature. The three bfta ligands have phenyl and $CF_3$ substituents and the Py-Im ligand coordinates through N-atoms of a five and a six-membered ring. The ligands are orientated such that the three $CF_3$ groups from the three bfta ligands sit on the same side of the molecule as the pyridine ring of the Py-Im ligand, and the point group of the molecule is best described as $C_S$.

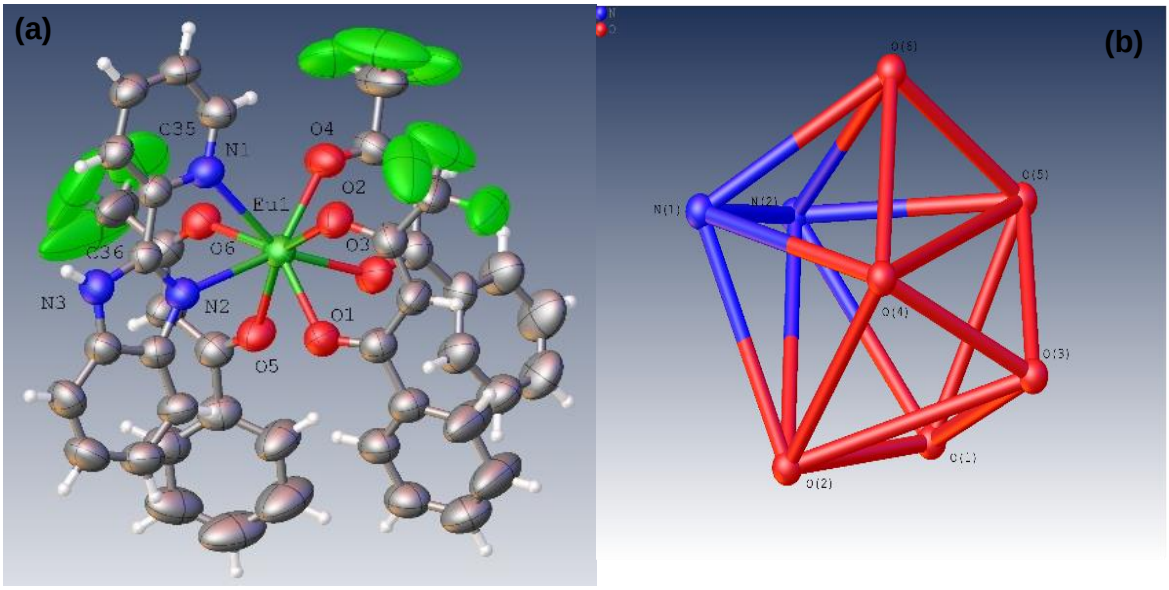


**Fig. 1.** (a) The molecular structure of **Eu-1** showing the selected atom numbering. The displacement ellipsoids have been drawn with 50% probability. Selected Eu-ligand bond distances (Å) are as follows: Eu(1)-O(1) 2.415(3), Eu(1)-O(2) 2.443(3), Eu(1)-O(3) 2.346(3), Eu(1)-O(4) 2.352(3), Eu(1)-O(5) 2.351(3), Eu(1)-O(6) 2.358(3), Eu(1)-N(1) 2.620(4), Eu(1)-N(2) 2.529(3). (b) The ligand coordination polyhedron showing the trigonal dodecahedral arrangement of the $O_6N_2$ bridgehead atoms.

In **Eu-1** the Eu-O bond distances range from 2.346(3) to 2.443(3) Å while the two Eu-N bond distances are slightly longer ranging from 2.529(3) to 2.620(4) Å, reflecting a slightly asymmetric bonding of the Py-Im ligand. The Eu-O bond lengths for the bfta ligand that contains the O(1) and O(2) bridgehead atoms are significantly longer, by *ca*. 0.07 Å, than the bond lengths for the other two pairs of Eu-O bonds. The asymmetry in the Eu-O bonds lengths for each bfta ligand is less than 0.01 Å. The average Eu-O (2.38 Å) and Eu-N (2.58 Å) distances are similar to the average Eu-O (2.39 Å) and Eu-N (2.58 Å) distances obtained from the structures of over 1000 hits reported in the Cambridge Structural Database for eight coordinate Eu complexes with O- or N-donor ligands (Version 5.41 + 1 update).[12] The bond parameters within the Py-Im ligand all fall within the expected ranges and effectively planar with the N(2)-C(36)-C(35)-N(1) torsion angle being -0.8(6)°.

It is of interest to compare the structure of **Eu-1** to that of the closely related europium(III) complex **Eu-2 (Chart S1, ESI)** recently reported by us.[5] While the continuous

shape measure values (**Table S9, ESI**) show that both structures are best described as having a distorted trigonal dodecahedral coordination geometry. It is clear that the coordination environment in **Eu-2** corresponds more closely to the idealised trigonal dodecahedron than for **Eu-1**. An overlay of the two structures is shown in **Fig. S2, ESI** where the Eu atoms and the Py-Im ligands are directly overlayed. It is clear that the arrangement of the three hexafluoroacetylacetonate ligands is somewhat different in the two molecules. Distortions from idealised coordination geometries in lanthanide complexes with high coordination numbers is not uncommon and reflects the similarities in energies of the various coordination arrangements.[13] However, it has been reported previously that the coordination geometry adopted does have an influence on the luminescent emission quantum yields of Eu(III) and Sm(III) complexes; complexes with the trigonal dodecahedral arrangement having higher values [1c, 14]. Moreover, the ground state geometry of **Eu-1** was optimised from the crystallographic coordinates (details are included in the ESI and optimized structure is shown in **Fig. S3, ESI)**. The comparison among the geometries optimized by different density functional theory (DFT) methods with the crystallographic geometry is shown in **Fig. S4, ESI.** Root mean square deviations and the spherical atomic coordinates are listed in **Tables S10 and S11, ESI**. The PBE1PBE functional gave reasonable agreement with the structure determined by X-ray analysis and this agreement did not improve when a higher level of theory was used, so optimisation was performed using the PBE1PBE level of theory.

### 3.2. Experimental and theoretical photophysical properties of Eu-1

The optical absorption spectrum of **Eu-1** was obtained in $CH_2Cl_2$ (DCM) solution ($1 \times 10^{-5}$ M) and is shown in **Fig. 2a**. The electronic spectrum exhibits a broad transition in the range between 270 nm and 400 nm with $\lambda_{max}^{abs}$ = 313 nm and could be assigned to π-π* transition due to both the primary β-diketonate ligand and the ancillary ligand ($\lambda_{max}^{abs}$ = 310 nm for free Py-IM) [5]. To present a clearer picture and to understand this observation better, we calculated the electronic spectrum of **Eu-1** by the TD-DFT method (Please see the details in the ESI). The theoretical absorption spectra obtained using the CAM-B3LYP, ωB97X-D3BJ and M06-2X

functionals from the PBE1PBE geometry are shown in **Fig. 2b**. The use of CAM-B3LYP was motivated by the interesting qualitative results obtained in our previous work [4]. In addition to this, ωB97X-D3BJ was also included to evaluate the results of a functional containing both dispersion and long-range interactions. As was noted by Jacquemin and co-workers, the M06-2X functional provided the best agreement with experimental data for singlet-triplet transition energies among 30 density functions evaluated [15]. We also tested this functional for the present complex.

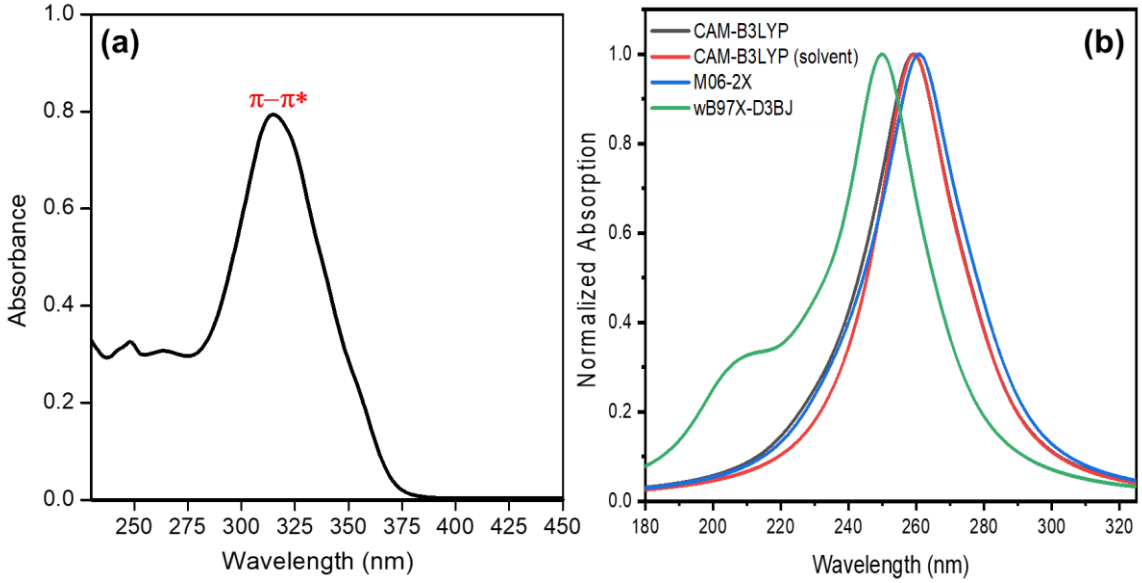


**Fig. 2**. (a) UV-Visible absorption spectrum of **Eu-1** in DCM solution at RT. (b) Theoretical absorption spectra calculated using the TD-DFT methods with the CAM-B3LYP, M06-2X and ωB97X-D3BJ functionals.

The spectra calculated by CAM-B3LYP and M06-2X both underestimated $\lambda_{max}^{abs}$ = 260 nm. However, the spectra are identical, indicating a good agreement for their corresponding energy of the singlet of highest oscillator strength. Moreover, **Fig. 2b** reveals that the implicit inclusion of the DCM solvent in the calculation did not yield any change in the position of the most intense transition and its shape. A plausible explanation of this observation could be because of the small value of the dielectric constant of DCM (*ca.* 9.0). Although the absorption spectrum obtained at the ωB97X-D3BJ level contains a band in the region of lower wavelengths, the method further underestimates $\lambda_{max}^{abs}$ (*ca.* 250 nm) and thus overestimates the energy of the singlet exited states. For all density functionals applied in the TD-DFT

calculations, the analysis of the electronic transitions involved in the composition of the singlet state of highest oscillator strength indicated that the most relevant MOs are within of the range of HOMO-4 to LUMO+3. **Fig. 3** shows the MOs in this range calculated at the CAM-B3LYP/SVP/MWB52 level of theory and it is noted that both primary (btfa) and ancillary (Py-Im) ligands contribute to the most intense absorption as noted experimentally. This observation is further corroborated by the natural transition orbitals (NTOs) analysis at the same level of theory (**Fig. S5, ESI**), from which a simple representation of the transition density between the ground and the excited state is obtained [16].

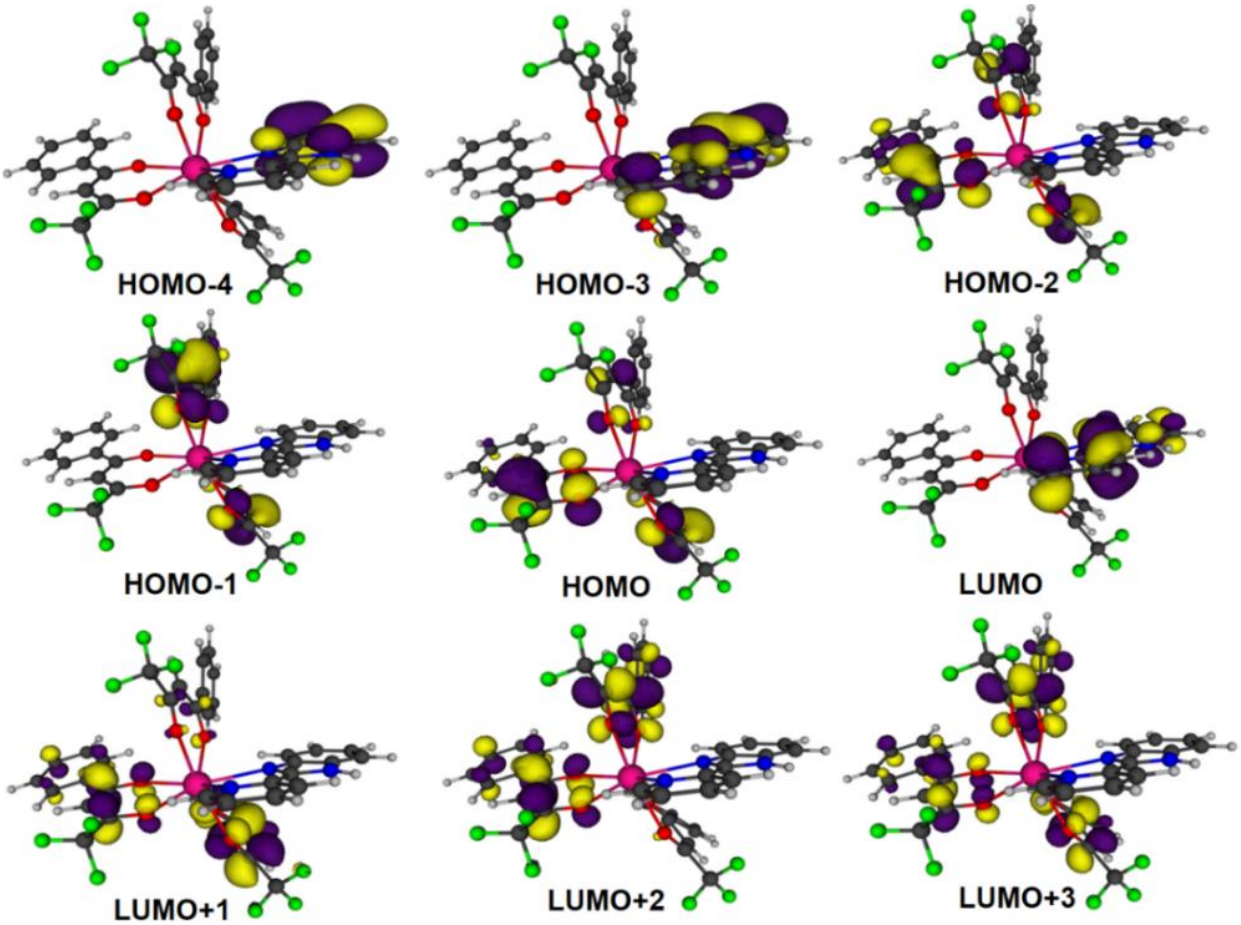


**Fig. 3.** MOs within of the range of HOMO-4 to LUMO+3, which were calculated with the TD-DFT CAM-B3LYP/SVP/MWB52 method using the PBE1PBE geometry.

The steady-state PL (excitation and emission) properties of **Eu-1** were determined in the solid-state and in DCM solution ($1 \times 10^{-5}$ M). Excitation spectra in both cases displayed a broad transition in the range 300 – 400 nm and could be attributed to π-π* transition of both the btfa and Py-Im ligands (**Fig. S6 & S7, ESI**). Moreover, the spectrum in the solid-state does show

some intra-configurational f–f transitions. The emission in the solid-state and in DCM solution was obtained by exciting it at $\lambda_{max}^{ex}$ depicted in **Fig. 4** and **Fig. S8, ESI**. The spectra in each case displayed five well-resolved emission transitions of Eu(III); these are assigned to $^5D_0 \rightarrow {}^7F_0$, $^5D_0 \rightarrow {}^7F_1$, $^5D_0 \rightarrow {}^7F_2$, $^5D_0 \rightarrow {}^7F_3$ and $^5D_0 \rightarrow {}^7F_4$, respectively [4b, 17]. The barycentre of the transitions, intensities relative to the magnetic dipole (MD) $^5D_0 \rightarrow {}^7F_1$ transition and % contribution of each transition are provided in **Table S12, ESI**. The spectrum in either case is dominated by the electric dipole (ED) $^5D_0 \rightarrow {}^7F_2$ transition that contributes 81% of the total integral intensity (**Table S12, ESI)**. Consequently, **Eu-1** exhibits pure red emission (full width at half maxima (FWHM) = $(3.00\ nm)_{solid\text{-}state}$ and $(3.90\ nm)_{DCM}$, **Table 2**) with CIE color coordinates $(0.668, 0.331)_{solid\text{-}state}$ and $(0.668, 0.332)_{DCM}$ (**Table 1** and **Figs. S9 & S10, ESI**). The CIE color coordinates are very similar to NTSC: x – 0.67; y – 0.33, implying the potential of the present **Eu-1** as a dopant to fabricate red OLEDs.

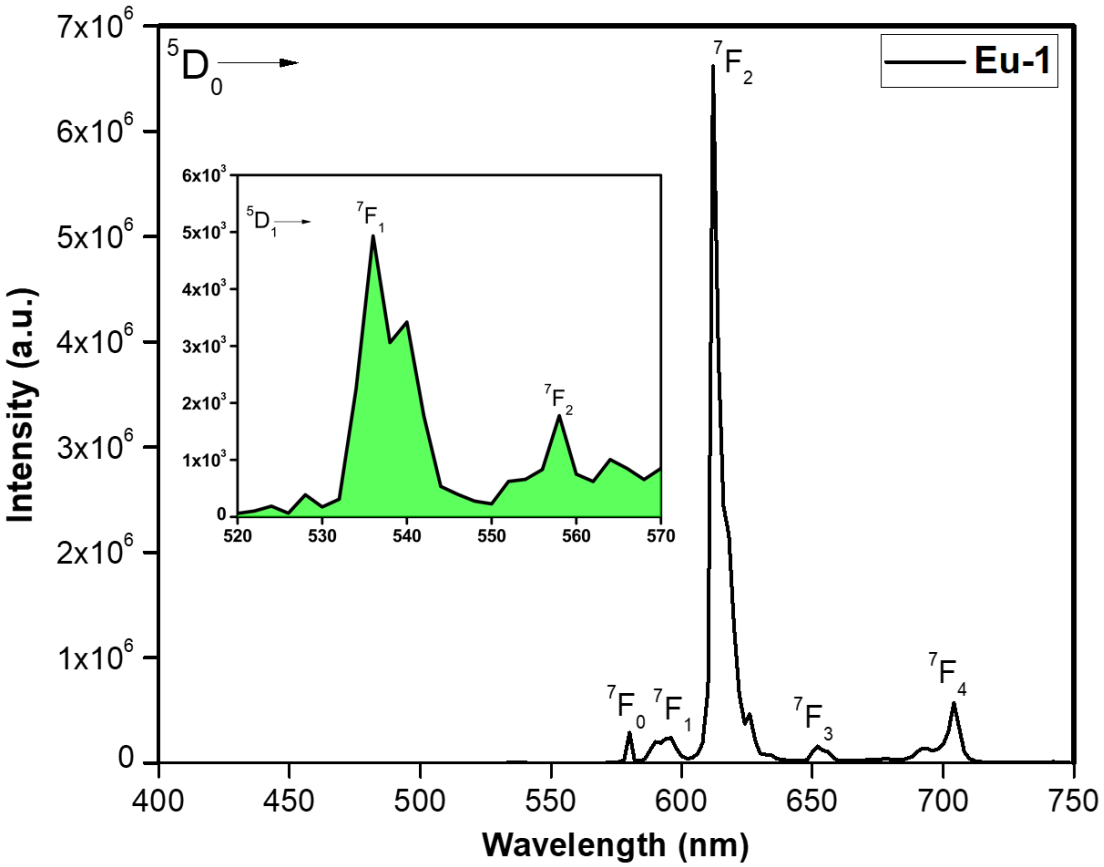


**Fig. 4**. Corrected emission spectrum of **Eu-1** in DCM solution at RT. Inset showing the magnification of the region between 500 – 570 nm displaying $^5D_1 \rightarrow {}^7F_{1,2}$ transitions.

Lifetimes ($\tau_{obs}$) in the solid-state and in DCM solution for **Eu-1** were determined by fitting the decay curves (**Figs. S11 & S112, ESI**) and the data obtained are presented in **Table 1**. The decay curves either in the solid-state or in DCM solution fit well with monoexponential ($\chi^2$ = 0.995 – 1.023) behavior and confirm the presence of a single dominant emitting species in both states. This further corroborates the results of the steady-state emission spectra where the $^5D_0 \rightarrow {}^7F_0$ emission transition displayed a single unsplit peak with a 1.26 – 1.47 % contribution to the total integral intensity (**Table S12, ESI)**. **Eu-1** in both the states exhibits long $\tau_{obs}$ (**Table 1**) and are in the range of typical europium β-diketonate complexes with N^N ancillary ligand. Moreover, we utilized the steady-state emission spectra and $\tau_{obs}$ of **Eu-1** to determine the important photophysical parameters; $\Omega_2$ and $\Omega$ parameters, $A_R$ and $A_{NR}$ decay rates, $\tau_{rad}$ , $Q_{Eu}^{Eu}$ and $\eta_{sen}$ , respectively, using equations S1 – S7. The results obtained are shown in **Table 1**. The complex displayed large $\Omega_2$ = (27.94 × $10^{-20}$ $cm^2$)$_{solid\text{-}state}$ attributed to the distortion of coordination sphere from idealised trigonal dodecahedral caused by the presence of the unsymmetrically coordinated ligands (molecular point group $C_S$), which further corroborates with the large $R_{21}$ (**Table 1).** The $\Omega_2$ value of **Eu-1** is higher than that of **Eu-2** ( $\Omega_2$ = 23.90 ×$10^{-20}$ $cm^2$) [5] which could be attributed to higher distortion in the coordination geometry around Eu(III) for **Eu-1** (CShMs = 0.997) than **Eu-2** (CShMs = 0.745). Furthermore, the parameter $\Omega$ is closely related to the covalency of Ln-X bonds [18] (X is an atom in the coordination polyhedron) and long-range effects (hydrogen bonding, π–π stacking). The large $\Omega$ value (6.96 ×$10^{-20}$ $cm^2$) is consistent with the presence hydrogen bonding in the solid-state, which is confirmed by the single crystal structure that shows N—H···O hydrogen bonding. Moreover, the $\Omega$ value of **Eu-1** is quite similar to that of **Eu-2** ( $\Omega$ = 6.87 ×$10^{-20}$ $cm^2$) [5] having similar hydrogen bonding and covalency of the Eu-X bonds and is consistent with our observation. **Eu-1** displayed a large value of the absolute $Q_{Eu}^{L}$ = 40.8 in the solid-state and 44.4% in solution, respectively. The higher value in the solution phase could be due to a smaller value of $A_R$ = 228.24 $s^{-1}$ compared to solid-state 465.38 $s^{-1}$ (**Table 2**). The zero differential overlap (ZDO) electronic densities and the electrophilic superdelocalizabilities

calculated by the RM1 model using the PBE1PBE geometry for the atoms of the coordination polyhedron for **Eu-1**, along with charge factors (*g*) and polarizabilities (*α*) calculated by using the *QDC* model, are shown in **Table S13, ESI**. A *D/C* value greater that one is indicative of the fitting procedure provided intensity parameters are well reproduced and this is the case for the present complex. The low value of the intensity parameters *via* forced electric dipole ( $\Omega_{\lambda}^{FED}$ ) suggests that the emission of the Eu(III) ion is governed by the dynamic coupling (DC) mechanism. As a result, $\Omega_{\lambda}$ weakly depends on the charge factors of the atoms directly connected to Eu(III).

**Table 1**. Experimental and theoretical photophysical parameters of **Eu-1** in the solid-state and DCM solution at RT.

| | $\Omega_2$ | $\Omega$ | FWHM[b] | $\tau_{obs}$ | $\tau^{c}_{rad}$ | $A^{d}_{R}$ | $A^{e}_{NR}$ | $(Q^{Eu}_{Eu})$[f] | $Q^{L}_{Eu}$ | $\eta^{g}_{sen}$ | $R^{h}_{21}$ | CIE (x,y) |
|---|---|---|---|---|---|---|---|---|---|---|---|---|
| | ×$10^{-20}$ $cm^2$ | | | (μs) | | ($s^{-1}$) | | (%) | | (%) | | |
| | **Solid-state** | | | | | | | | | | | |
| **Eu-1** | 27.94[a] | 6.96[a] | 3.00 | 660±1.36 | 965.13 | 1036.12 | 465.38 | 69.01 | 40.8 | 59.12 | 15.96 | 0.668, 0.331 |
| **Eu-2 [5]** | 23.90 | 6.87 | | 833.01 | 1120 | 892.71 | 307.77 | 74.36 | | | 13.75 | 0.668, 0.330 |
| | **DCM** | | | | | | | | | | | |
| **Eu-1** | 26.95 | 7.57 | 3.90 | 921±2.15 | 1164.53 | 858.71 | 228.24 | 79.00 | 44.4 | 56.20 | 15.45 | 0.668, 0.332 |
| **Theoretical** | 26.96 | 7.57 | - | - | 1205.10 | 829.81 | 255.97 | 76.43 | 42.8 | 56.11 | - | - |

[a] calculated using equation S1; [b] FWHM of ED $^5D_0 \rightarrow {}^7F_2$ transition; [c] calculated using equation S5; [d] calculated using equations S2 and S3; [e] calculated using equation S4; [f] calculated using equation S6; [g] calculated using equation S7; [h] ratio of $^5D_0 \rightarrow {}^7F_2/{}^5D_0 \rightarrow {}^7F_0$ (**Section 1.1, ESI**)

### 3.3. Ligand-lanthanide ion ET for Eu-1

In order to discuss the main ET pathways that are operative in **Eu-1**, the results obtained at the CAM-B3LYP level of theory are investigated. An analysis of the MOs reveals that the triplet state of the btfa ($T_1$ = 22972 $cm^{-1}$, $T_2$ = 23054 $cm^{-1}$ and $T_3$ = 23170 $cm^{-1}$) and Py-Im ($T_4$ = 26354.0 $cm^{-1}$) are involved in ET processes with the dominant character coming from the $T_1$ and $T_4$ states. It is important to note that btfa triplet states ($T_1$ – $T_3$) are practically degenerate and involve a contribution from the different btfa ligands; therefore, we have considered only the $T_1$ state. Thus, most important electronic transitions for the composition of $S_1$, $T_1$, and $T_4$ are listed in **Table 2**. As mentioned in the introduction, the experimentally determined first triplet states of the btfa and Py-Im ligands lie at 21,400 $cm^{-1}$ [3b] and 20,576 $cm^{-1}$ [5], respectively. However, the results of TD-DFT indicates that the first triplet state of Py-Im is not dominant; instead, it is the $T_4$ [HOMO-3 → LUMO transition (71.11%)] of Py-Im.

**Table 2:** Energy of the singlet and triplet excited states considered in the process of ET, distance from energy donor to acceptor centre ($R_L$), and electronic transition configurations calculated at the TD-DFT CAM-B3LYP level of theory for the corresponding triplet state of **Eu-1**.

| State | Energy ($cm^{-1}$) | $R_L$ (Å) | Major Contribution | Total (%) |
|---|---|---|---|---|
| $S_1$ | 33,732.4 | 4.1691 | HOMO-12→LUMO+1 (21.50%)<br>HOMO-6→LUMO+1 (13.54%)<br>HOMO-12→LUMO+3 (11.44%)<br>HOMO-11→LUMO+1 (8.03%)<br>HOMO-9→LUMO+1 (7.03%)<br>HOMO-6→LUMO+3 (6.24%) | 67.78 |
| $T_1$ | 22,971.8 | 4.2671 | HOMO→LUMO+1 (25.58%)<br>HOMO-1→LUMO+1 (18.85%)<br>HOMO-2→LUMO+3 (10.11%)<br>HOMO-2→LUMO+1 (8.56%)<br>HOMO→LUMO+3 (8.46%)<br>HOMO-1→LUMO+3 (6.58%) | 78.14 |
| $T_4$ | 26,354.0 | 4.3517 | HOMO-3→LUMO (71.11%) | 71.11 |

In order to consider the contribution from both the ligands, the ET rates involving $T_1$ and $T_4$ states were taken into account for calculating the energetic population of each state considered in the schematic energy-level diagram for **Eu-1** illustrated in **Fig. 5**. Regarding the

$S_1$ state, **Table S14, ESI** shows that the largest value of ET rate is of the order of $10^5$ $s^{-1}$ and are associated with the $^7F_1 \rightarrow {}^5G_2$ and $^7F_1 \rightarrow {}^5G_3$ acceptors, where the former is governed by the direct Coulomb interaction (CI) mechanism and the latter by the exchange (Ex.) mechanism. The ET pathways from the $T_1$ state to $^5D_0$ and $^5D_1$ are the most relevant for the sensitization of the Eu(III) emission. Both the $^7F_0 \rightarrow {}^5D_1$ and $^7F_0 \rightarrow {}^5D_1$ acceptors have ET rates of the order of $10^7$ $s^{-1}$ and these pathways are governed by the Ex. mechanism ($\Delta J = 1$). In case of $T_4$, it is noted that the pathways related to $^7F_0 \rightarrow {}^5D_1$ and $^7F_0 \rightarrow {}^5D_1$ also have appreciable values of rate of the order of $10^6$ $s^{-1}$. Interestingly, because of the extreme resonance condition between $T_4$ and $^5G_2$ ($\Delta$ = 38 $cm^{-1}$), the backward ET rate and the forward ET rate are of the same order of magnitude ($10^7$ $s^{-1}$) (**Table S14, ESI**). **Table S14** also reveals that for some pathways related to $T_1$ large values of backward ET rates are provided. For these cases, it should be noted that the states of Eu(III) involved are considerably above $T_1$ and such fast pathways return the energy to $T_1$ so that it can be transferred to more resonant states of Eu(III).

The experimental $\eta_{sen}$ for **Eu-1** is 56.2% in DCM solution. Such a result suggests that additional pathways that depopulate the triplet states are operative and, as a result, an expressively shortening of the emission lifetime occurs, increasing the value of their corresponding decay rates. This fact is contemplated in the Jablonski diagram (**Fig. 5**) for **Eu-1** in which it is necessary to take values for the decay rates involving the $T_1$ and $T_4$ states of the order of $10^7$ $s^{-1}$ to reproduce the experimental $\eta_{sen}$. The theoretical $Q_{Eu}^{L}$ , $Q_{Eu}^{Eu}$ and $\eta_{sen}$ obtained are 42.8%, 76.4% and 56.0% calculated using the PBE1PBE/SVP/MWB52 level of theory (**Table 1**), and thus reproduce the experimental photophysical parameters. Furthermore, tests have shown that the inclusion of other states of Eu(III) besides those usually considered ($^5D_4$, $^5D_1$, and $^5D_0$) [4] does not alter the magnitude of the decay rates, once the excitation of Eu(III) arises mainly due to the ET pathways involving the $^5D_1$ and $^5D_0$ states. Therefore, the simplest case is considered to illustrate a schematic energy-level diagram for **Eu-1**.

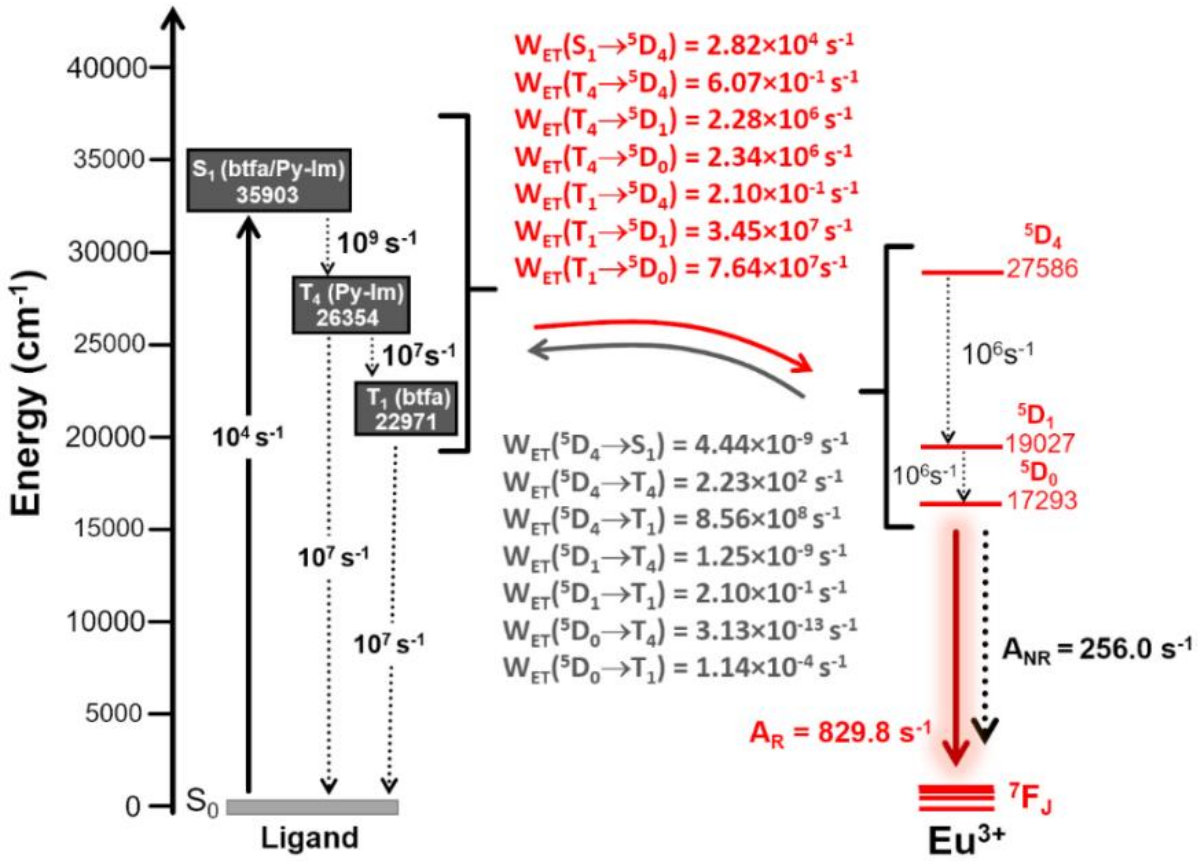


**Fig. 5.** Schematic energy-level diagram for **Eu-1**, showing the corresponding rate for the ET pathways most important calculated using models proposed by Malta.

### 3.4. EL studies of Eu-1

Before undertaking device fabrication by thermal evaporation of **Eu-1**, it is necessary to determine its thermal stability because low $T_d$ for any complex would certainly lead to depletion in its OLED performance. The complex exhibits a high $T_d$ = 286 °C at a weight loss of 5% (**Fig. 6**). Moreover, the DTA of the complex shows an endothermic peak at 220 °C representing the melting point of **Eu-1 (Fig S13, ESI)**.

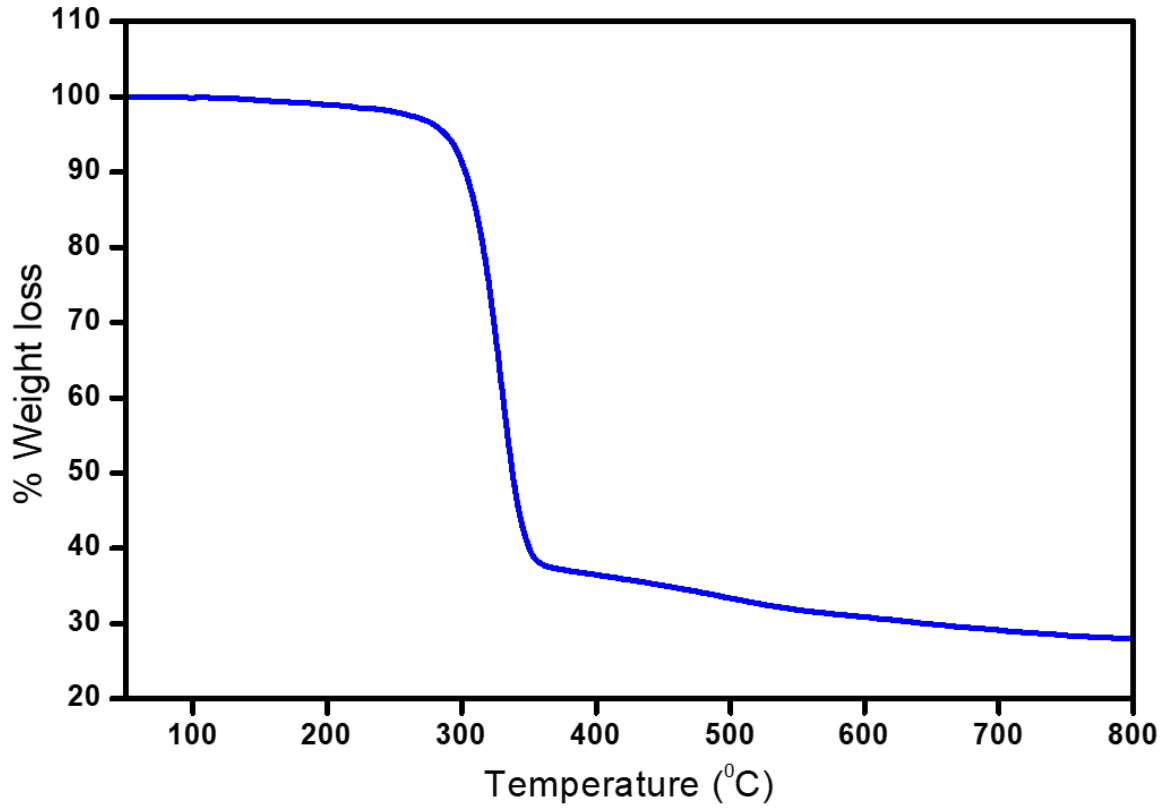


**Fig. 6**. TGA profile of **Eu-1** under a dinitrogen atmosphere.

Promising PL properties (Table 1) coupled with the high thermal stability of **Eu-1** implies that the complex could be utilized as an EML to fabricate red OLED. To test this, we have utilized **Eu-1** as an EML to fabricate the single- and double EML devices as shown in **Chart 1 (Section 3, ESI)**. The OLEDs were fabricated by the thermal evaporation and the concentration of the complex was adjusted to be 3.0 wt%, 4.0 wt%, 5.0 wt% and 6.0 wt%, respectively. As the doping concentration increases, the evaporation temperature increases gradually from 115 to 139 °C. It is important to mention that the low sublimation temperature of **Eu-1** warrants negligible decomposition of the complex during the thermal evaporation process.

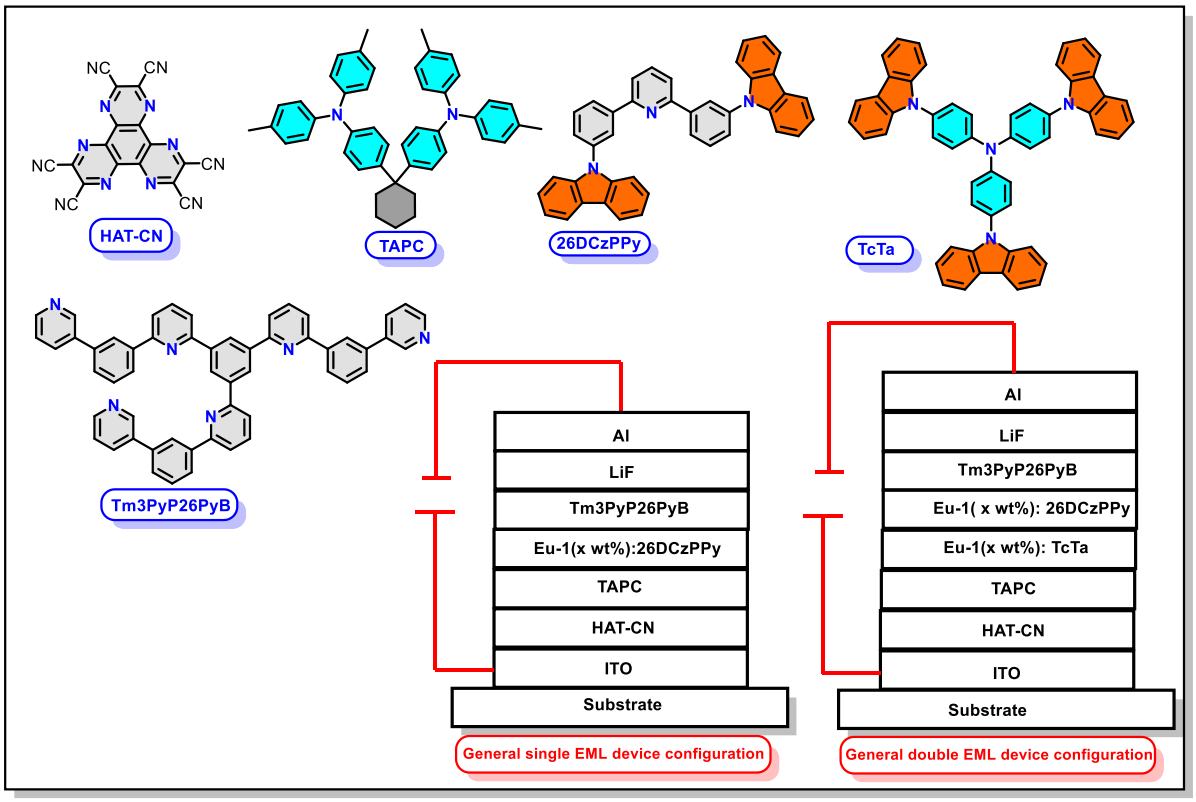


**Chart 1**: Molecular structures of the compound and general device configuration.

The normalized EL spectra of **Eu-1** based single- and double EML OLEDs are shown in **Fig. 7a** and **Fig. S14, ESI**. The EL spectra of the single EML devices (**Fig. S14, ESI**) show a well resolved emission that compares well with the PL spectra of **Eu-1** in the solid-state and in DCM solution and suggests that the recombination of electrons and holes were successfully confined to the Eu(III) complex layer. Moreover, the EL spectra of the devices exhibit host emission (350 – 500 nm); however, the intensity of this emission decreases as the doping concentration increases from 3 wt% to 6 wt% (**Fig. S14, ESI**). Theoretically speaking, more and more emitter molecules would participate in the EL processes with increasing doping concentration of emitter. As a result, ET from host to emitter molecules tends to be faster with increasing doping concentration of emitter because of the shorter molecular distance between emitter molecules. So, the reduction of the host emission intensity from device **1** to device **4** implies improved ET from the host materials to **Eu-1.** The color of the device changed from magenta (device **1**; (CIE)x,y = 0.570, 0.280, **Table 4**, **Fig. S10**, **ESI**) to red (device **3**; (CIE)x,y = 0.634, 0.308, **Table 4**, **Fig. S10**, **ESI**). As shown in **Fig. 7a,** the double EML devices (devices

**5** – **8**) exhibit similar decreased host emission with the doping concentration. In this case, the very minor host emission at 390 nm could be attributed to that of the TcTa emission which decreases as the doping concentration increases. This suggests that both carrier trapping and Förster ET are taking part in the device luminescence process [7, 19]. The devices display pure red EL as can be seen in **Fig. 7b**. Compared to the single-EML devices, the double-EML devices show relatively weaker host emission and imply a wider recombination zone that facilitates the ET from the host to the **Eu-1** because more Eu(III) molecules participate in the EL processes.

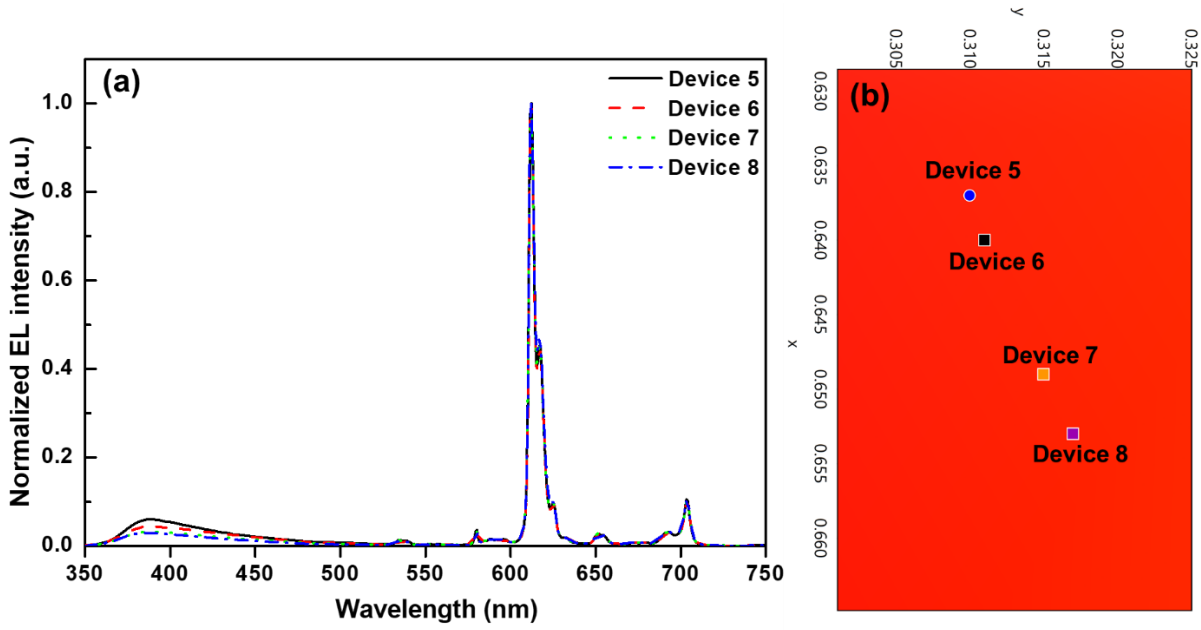


**Fig. 7**. (a) Normalized EL spectra of device **5**, **6**, **7** and **8** and (b) magnified view of CIE 1931 chromaticity diagram of the respective devices operating at 10 mA/cm$^2$.

**Table 3**: Key properties of single- and double- EML EL devices of **Eu-1**.

| | $V_{turn\text{-}on}$ (V) | B[a] (cd/m$^2$) | $\eta_c$[b] (cd/A) | $\eta_p$[d] (lm/W) | EQE(%)[c] | $CIE_{x,y}$[e] |
|---|---|---|---|---|---|---|
| **Single EML Devices** | | | | | | |
| **Device 1** | 3.3 | 1103 | 1.77 | 1.68 | 1.3% | 0.570, 0.280 |
| **Device 2** | 3.4 | 1175 | 1.84 | 1.60 | 1.3% | 0.618, 0.302 |
| **Device 3** | 3.4 | 814 | 1.87 | 1.73 | 1.3% | 0.634, 0.308 |
| **Device 4** | 3.3 | 743 | 1.71 | 1.68 | 1.2% | 0.625, 0.305 |
| **Double EML Devices** | | | | | | |
| **Device 5** | 3.3 | 970 | 1.89 | 1.69 | 1.3% | 0.637, 0.310 |
| **Device 6** | 3.4 | 896 | 2.26 | 1.92 | 1.6% | 0.640, 0.311 |
| **Device 7** | 3.4 | 670 | 2.15 | 1.83 | 1.5% | 0.649, 0.315 |
| **Device 8** | 3.3 | 758 | 1.97 | 1.77 | 1.4% | 0.653, 0.317 |

[a] The data for maximum brightness (B), [b] maximum current efficiency ($\eta_c$), [c] maximum external quantum efficiency (EQE), [d] maximum power efficiency ($\eta_p$); [e] $CIE_{x,y}$ at 10 mA/cm$^2$

The EL efficiency and current density curves together with the voltage (V)–brightness (B) and current density curves are shown as an inset in **Fig. 8** and the detailed performance of the devices **1** – **8** are tabulated in **Table 3**. The single-EML device **3** (5 wt%) displayed impressive red EL ($CIE_{x,y}$ = 0.634, 0.308) with B = 814 cd/m$^2$, $\eta_c$ = 1.87 cd/A, $\eta_p$ = 1.73 lm/W and EQE = 1.3% at very low $V_{turn\text{-}on}$ = 3.4 V and current density 10 mA/cm$^2$. Double-EML devices displayed highly monochromatic red ($CIE_{x,y}$ = 0.637, 0.310 – 0.653, 0.317, **Table 3**, **Fig. 7b**) EL despite the presence of very faint host emissions which do not hamper the color purity of the device. At the optimium doping concentration i.e., Device **6** exhibits significantly improved B = 896 cd/m$^2$, $\eta_c$ = 2.26 cd/A, $\eta_p$ = 1.92 lm/W and EQE = 1.6% at very low $V_{turn\text{-}on}$ = 3.4 V. Moreover, $\eta_c$ increases from Device **5** to Device **6** and then started to decrease, which could be attributed to the imbalance between the hole-electron pair in the EML layer. Consequently, this will break the balance between the hole-electron pairs in EML and thus will lead to the decrease of the $\eta_c$ of device [20]. As shown in Fig. S14, ESI, PL delay characteristics of **Eu-1** film, **Eu-1** (4 wt %):26DCzPPy film, and **Eu-1** (4 wt%):TcTa film were measured and compared. In this case, the relatively longer excited lifetimes of Eu(III) emission in Eu-1 (4 wt%):26DCzPPy (718.1 μs) and Eu-1 (4 wt%):TcTa (674.3 μs) films compared with that in Eu-1 (565.5 μs) film can be attributed to the increased molecular distance and the presence of ET from 26DCzPPy or TcTa to **Eu-1** molecules. It is important to note that these EL performances were obtained at

a low $V_{turn-on}$ (3.3 – 3.4 V) implying a barrier-free carrier injection, balanced carrier transport and recombination and at the same time high ET efficiency from the exciplex host to **Eu-1**. The device based on **Eu-1** exhibited improved performance (**Table 4**) than the analogous europium complexes reported in the literature [5-9].

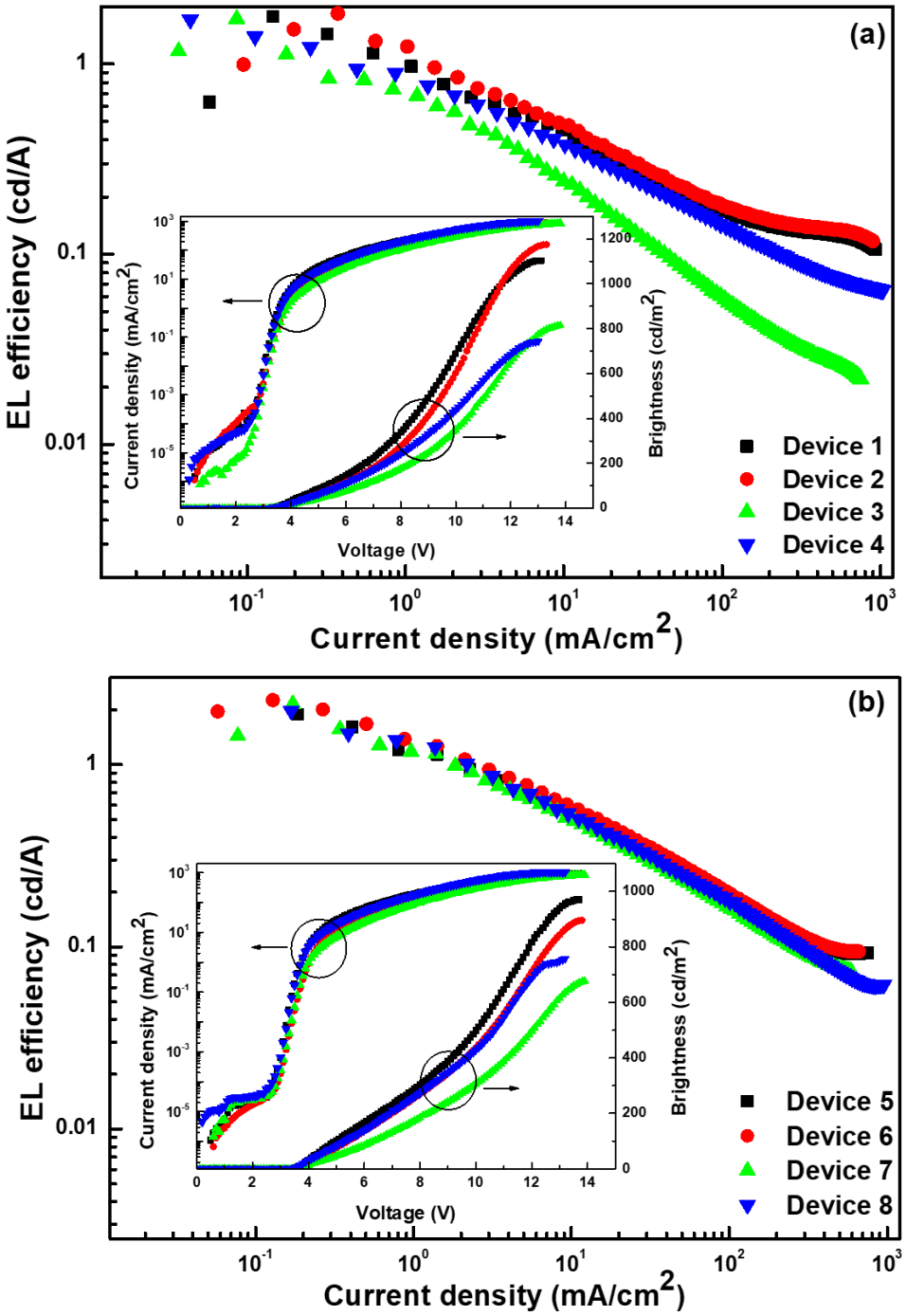


**Fig. 8**. EL efficiency-current density characteristics. Inset: Current density-brightness-voltage characteristics (a) Device **1**, **2**, **3** and **4** and (b) Device **5**, **6**, **7** and **8**.

**Table 4**: EL performance of the analogous europium complexes reported in the literature.

| | $V_{turn-on}$ (V) | B ($cd/m^2$) | $\eta_c$ (cd/A) | $\eta_p$ (lm/W) | EQE(%) |
|---|---|---|---|---|---|
| **Eu-1** | 3.4 | 896 | 2.26 (10 mA/ | 1.92 | 1.6 |
| **Eu-2 [5]** | 4.4 | 328 | $cm^2$) 0.47 (10 | 0.33 | 0.07 |
| $[Eu(dbm)_3(EPy\text{-}Im)]$ [6] | | 180 (18V) | $mA/cm^2$) | 0.05 (10V) | |
| $[Eu(dbm)_3(Ox\text{-}Py\text{-}Im)]$ [7] | | 322 (21V) | 1.9(21V) | | 1.7 |
| $[Eu(dbm)_3(Car–Py\text{-}Im)]$ | | 200 (20V) | 4.2 (0.5 $mA/cm^2$) | | |
| [8] $[Eu(tta)_3(EPy\text{-}Im)]$ [9] | | 36.6 (21V) | | | |

EPy-Im= 1-ethyl-2-(2-pyridyl)benzimidazole

## 4. Conclusion

In summary, we have synthesized a new mixed-ligand europium(III) complex **Eu-1** by following a two-step synthetic methodology. A single-crystal X-ray diffraction experiment showed that **Eu-1** is eight coordinate with a highly distorted trigonal dodecahedral ($D_{2d}$) coordination geometry. Thermogravimetric analysis showed that **Eu-1** possesses high thermal stability with $T_d$ = 286 °C and is therefore an excellent candidate for OLED fabrication by the thermal evaporation method. The complex displayed highly monochromatic red emission in solid-state and in solution with large $Q_{Eu}^{L}$ (**Table 1**). An ET mechanism from ligand to Eu(III) is proposed with the help of TD-DFT calculation and LUMPAC software package (https://lumpac.pro.br/). It was observed that the triplet states of both the primary (btfa) ligand and the ancillary (Py-Im) ligand take part in the ET process. Moreover, it is important to emphasize that the first triplet state of the ancillary Py-Im ligand is not the dominant triplet state in the ET process, rather it is the fourth triplet state (26,354 $cm^{-1}$), which is uncommon in this type of europium complex. Finally, we have demonstrated the potential application of the complex as an EML to fabricate bright and monochromatic red OLEDs. The double-EML device at the optimum doping concentration exhibited B = 896 $cd/m^2$, $\eta_c$ = 2.26 cd/A, $\eta_p$ = 1.92 lm/W and EQE = 1.6% at very low $V_{turn-on}$ = 3.4 V at current density 10 $mA/cm^2$ and $(CIE)_{x,y}$ = 0.640, 0.311, thus proving its strong candidature as one of the components in portable full color flat display. The

device based on **Eu-1** displayed improved EL performance than the analogous europium complexes (Table 4) reported in the literature [5-9].

## Conflicts of interest

The authors declare no conflicts of interest.


## Acknowledgements

MSK acknowledges His Majesty's Trust Fund for Strategic Research (Grant No. SR/SQU/SCI/CHEM/21/01) for funding. RI thanks HM's Trust Fund for a postdoctoral fellowship. JDLD appreciates the financial support from the Brazilian funding agencies: CAPES, CNPq (421733/2018-7), FACEPE (APQ - 0675-1.06/14) and FAPITEC-SE (Process N. 019.203.01074/2011-1). The computing for this project was performed on the LCAD-UFS (UFS High Performance Computing Laboratory). WYW thanks the Hong Kong Research Grants Council (PolyU 153058/19P), Guangdong-Hong Kong-Macao Joint Laboratory of Optoelectronic and Magnetic Functional Materials (2019B121205002), Hong Kong Polytechnic University (1-ZE1C) and the Endowed Professorship in Energy from Ms Clarea Au (847S) for the financial support. LZ is grateful to the financial aid from National Natural Science Foundation of China (21771172), Youth Innovation Promotion Association of Chinese Academy of Sciences (2013150). PRR is grateful to the Engineering and Physical Sciences Research Council (EPSRC) for continued funding (Grant EP/K004956/1).


## References


[1] (a) W. Liu, L. Zhou, L.Y. Jin, W. Xie, C.-M. Che, G. Cheng, Improved color quality in double-EML WOLEDs by using a tetradentate Pt(Ⅱ) complex as green/red emitter, J. Mater. Chem. C, (2021). https://doi.org/10.1039/D0TC05686C; (b) S. Wang, H. Zhang, B. Zhang, Z. Xie, W.-Y. Wong, Towards high-power-efficiency solution-processed OLEDs: Material and device perspectives, Mater. Sci. Eng., R, 140 (2020) 100547. https://doi.org/10.1016/j.mser.2020.100547; (c) R. Ilmi, M.S. Khan, W. Sun, L. Zhou, W.-Y. Wong, P.R. Raithby, A single component white electroluminescent device fabricated from a metallo-organic terbium complex, J. Mater. Chem. C, 7 (2019) 13966-13975. https://doi.org/10.1039/C9TC04653D; (d) S. Hirata, Y. Sakai, K. Masui, H. Tanaka, S.Y. Lee, H. Nomura, N. Nakamura, M. Yasumatsu, H. Nakanotani, Q. Zhang,

K. Shizu, H. Miyazaki, C. Adachi, Highly efficient blue electroluminescence based on thermally activated delayed fluorescence, Nat. Mater., 14 (2014) 330. https://doi.org/10.1038/nmat4154; (e) S. Kim, H.-J. Kwon, S. Lee, H. Shim, Y. Chun, W. Choi, J. Kwack, D. Han, M. Song, S. Kim, S. Mohammadi, I. Kee, S.Y. Lee, Low-Power Flexible Organic Light-Emitting Diode Display Device, Adv. Mater., 23 (2011) 3511-3516. https://doi.org/10.1002/adma.201101066; (f) Z.B. Wang, M.G. Helander, J. Qiu, D.P. Puzzo, M.T. Greiner, Z.M. Hudson, S. Wang, Z.W. Liu, Z.H. Lu, Unlocking the full potential of organic light-emitting diodes on flexible plastic, Nat. Photonics, 5 (2011) 753-757. https://doi.org/10.1038/nphoton.2011.259; (g) S. Reineke, F. Lindner, G. Schwartz, N. Seidler, K. Walzer, B. Lüssem, K. Leo, White organic light-emitting diodes with fluorescent tube efficiency, Nature, 459 (2009) 234. http://dx.doi.org/10.1038/nature08003

[2] (a) J.-C.G. Bünzli, Benefiting from the Unique Properties of Lanthanide Ions, Acc. Chem. Res., 39 (2006) 53-61. https://doi.org/10.1021/ar0400894; (b) O. Guillou, C. Daiguebonne, G. Calvez, K. Bernot, A Long Journey in Lanthanide Chemistry: From Fundamental Crystallogenesis Studies to Commercial Anticounterfeiting Taggants, Acc. Chem. Res., 49 (2016) 844-856. https://doi.org/10.1021/acs.accounts.6b00058; (c) E.G. Moore, A.P.S. Samuel, K.N. Raymond, From Antenna to Assay: Lessons Learned in Lanthanide Luminescence, Acc. Chem. Res., 42 (2009) 542-552. https://doi.org/10.1021/ar800211j; (d) L. Wang, Z. Zhao, C. Wei, H. Wei, Z. Liu, Z. Bian, C. Huang, Review on the Electroluminescence Study of Lanthanide Complexes, Adv. Opt. Mater., 0 (2019) 1801256. https://doi.org/10.1002/adom.201801256; (e) H. Xu, Q. Sun, Z. An, Y. Wei, X. Liu, Electroluminescence from europium(III) complexes, Coord. Chem. Rev., 293–294 (2015) 228-249. http://dx.doi.org/10.1016/j.ccr.2015.02.018

[3] (a) M. Latva, H. Takalo, V.M. Mukkala, C. Matachescu, J.C. RodriguezUbis, J. Kankare, Correlation between the lowest triplet state energy level of the ligand and lanthanide(III) luminescence quantum yield, J. Lumin., 75 (1997) 149-169. https://doi.org/10.1016/S0022-2313(97)00113-0; (b) S. Sato, M. Wada, Relations between Intramolecular Energy Transfer Efficiencies and Triplet State Energies in Rare Earth β-diketone Chelates, Bull. Chem. Soc. Jpn., 43 (1970) 1955-1962. https://doi.org/10.1246/bcsj.43.1955

[4] (a) M.S. Khan, R. Ilmi, W. Sun, J.D.L. Dutra, W.F. Oliveira, L. Zhou, W.-Y. Wong, P.R. Raithby, Bright and efficient red emitting electroluminescent devices fabricated from ternary europium complexes, J. Mater. Chem. C, 8 (2020) 5600-5612. http://dx.doi.org/10.1039/D0TC00749H; (b) R. Ilmi, W. Sun, J.D.L. Dutra, N.K. Al-Rasbi, L. Zhou, P.-C. Qian, W.-Y. Wong, P.R. Raithby, M.S. Khan, Monochromatic red electroluminescence from a homodinuclear europium(iii) complex of a β-diketone

tethered by 2,2'-bipyrimidine, J. Mater. Chem. C, 8 (2020) 9816-9827. http://dx.doi.org/10.1039/D0TC02181D

[5] R. Ilmi, M.S. Khan, Z. Li, L. Zhou, W.-Y. Wong, F. Marken, P.R. Raithby, Utilization of Ternary Europium Complex for Organic Electroluminescent Devices and as a Sensitizer to Improve Electroluminescence of Red-Emitting Iridium Complex, Inorg. Chem., 58 (2019) 8316-8331. https://doi.org/10.1021/acs.inorgchem.9b00303

[6] L. Huang, K.-Z. Wang, C.-H. Huang, F.-Y. Li, Y.-Y. Huang, Bright red electroluminescent devices using novel second-ligand-contained europium complexes as emitting layers, J. Mater. Chem., 11 (2001) 790-793. https://doi.org/10.1039/B006919L

[7] F. Liang, Q. Zhou, Y. Cheng, L. Wang, D. Ma, X. Jing, F. Wang, Oxadiazole-Functionalized Europium(III) β-Diketonate Complex for Efficient Red Electroluminescence, Chem. Mater., 15 (2003) 1935-1937. https://doi.org/10.1021/cm0257724

*[8] L. Zhang, T. Li, B. Li, B. Lei, S. Yue, W. Li, Synthesis and electroluminescent properties of a carbozole-functionalized europium(III) complex, J. Lumin., 126 (2007) 682-686. https://doi.org/10.1016/j.jlumin.2006.10.025*

*[9] L. Huang, K.Z. Wang, C.H. Huang, D.Q. Gao, L.P. Jin, Synthetic and electroluminescent properties of two novel europium complexes with benzimidazole derivatives as second ligands, Synth. Met., 128 (2002) 241-245. http://dx.doi.org/10.1016/S0379-6779(01)00656-7*

*[10] M. Pinsky, C. Dryzun, D. Casanova, P. Alemany, D. Avnir, Analytical methods for calculating Continuous Symmetry Measures and the Chirality Measure, J. Comput. Chem., 29 (2008) 2712-2721. https://doi.org/10.1002/jcc.20990*

*[11] D. Casanova, M. Llunell, P. Alemany, S. Alvarez, The Rich Stereochemistry of Eight-Vertex Polyhedra: A Continuous Shape Measures Study, Chem. Eur. J., 11 (2005) 1479-1494. https://doi.org/10.1002/chem.200400799*

*[12] C.R. Groom, I.J. Bruno, M.P. Lightfoot, S.C. Ward, The Cambridge Structural Database, Acta Crystallogr., Sect. B: Struct. Sci., 72 (2016) 171-179. https://doi.org/10.1107/S2052520616003954*

*[13] S.A. Cotton, P.R. Raithby, Systematics and surprises in lanthanide coordination chemistry, Coord. Chem. Rev., 340 (2017) 220-231. https://doi.org/10.1016/j.ccr.2017.01.011*

*[14] K. Miyata, T. Nakagawa, R. Kawakami, Y. Kita, K. Sugimoto, T. Nakashima, T. Harada, T. Kawai, Y. Hasegawa, Remarkable Luminescence Properties of Lanthanide* Complexes with Asymmetric Dodecahedron Structures, Chem. - Eur. J., 17 (2011) 521-528. https://doi.org/10.1002/chem.201001993

[15] D. Jacquemin, E.A. Perpète, I. Ciofini, C. Adamo, Assessment of Functionals for TD-DFT Calculations of Singlet−Triplet Transitions, J. Chem. Theory Comput., 6 (2010) 1532-1537. https://doi.org/10.1021/ct100005d

[16] R.L. Martin, Natural transition orbitals, J. Chem. Phys., 118 (2003) 4775-4777. https://doi.org/10.1063/1.1558471

[17] (a) R. Ilmi, S. Anjum, A. Haque, M.S. Khan, A new brilliant red emitting Eu(III) ternary complex and its transparent flexible and photostable poly(urethane) hybrid thin film for optoelectronic applications, J. Photochem. Photobiol., A, 383 (2019) 111968. https://doi.org/10.1016/j.jphotochem.2019.111968; (b) R. Ilmi, A. Haque, M.S. Khan, Synthesis and photo-physics of red emitting europium complexes: An estimation of the role of ancillary ligand by chemical partition of radiative decay rate, J. Photochem. Photobiol., A, 370 (2019) 135-144. https://doi.org/10.1016/j.jphotochem.2018.10.042

[18] R.T. Moura, A.N. Carneiro Neto, R.L. Longo, O.L. Malta, On the calculation and interpretation of covalency in the intensity parameters of 4f–4f transitions in Eu3+ complexes based on the chemical bond overlap polarizability, J. Lumin., 170 (2016) 420-430. https://doi.org/10.1016/j.jlumin.2015.08.016

[19] P.-P. Sun, J.-P. Duan, H.-T. Shih, C.-H. Cheng, Europium complex as a highly efficient red emitter in electroluminescent devices, Appl. Phys. Lett., 81 (2002) 792-794. https://doi.org/10.1063/1.1497714

[20] Z.-Q. Jiao, X.-M. Wu, Y.-L. Hua, M.-S. Dong, Y.-J. Su, L.-Y. Shen, S.-G. Yin, Improving efficiency of organic light-emitting devices by optimizing the LiF interlayer in the hole transport layer, Chin. Phys. B, 20 (2011) 107803. http://dx.doi.org/10.1088/1674-1056/20/10/107803